PHYSICS AND CHEMISTRY OF SOLID STATE
V. 25, No. 3 (2024) pp. 498-505
Section: Physics

DOI: 10.15330/pcss.25.3.498-505

Vasyl Stefanyk Precarpathian National University

ФІЗИКА І ХІМІЯ ТВЕРДОГО ТІЛА
Т. 25, № 3 (2024) С. 498-505
Фізико-математичні науки

PACS: 07.07.Df; 42.79.Pw

ISSN 1729-4428 (Print)
ISSN 2309-8589 (Online)

Erdal Turgut[1], Elvan Şenarslan[1], Günay Merhan Muğlu[2], Sevda Sarıtaş[3]

Assessment of titanium - tungsten iron oxide and their gas sensor application

[1]*Atatürk University, Department of Electric Power Generation, Aşkale Vocational College, Erzurum, Turkey*
[2]*Atatürk University, Department of Medical Services and Techniques, Hınıs Vocational School, Erzurum, Turkey*
[3]*Atatürk University, Department of Electric Power Generation, Transmission and Distribution, İspir Hamza Polat Vocational College, Erzurum, Turkey, sevda.saritas@atauni.edu.tr*

The titanium iron oxide ($Ti_xFe_{3-x}O_4$) and the tungsten iron oxide ($W_xFe_{3-x}O_4$) structures were grown by the RF-DC magnetron co-sputtering technique. When examining the atomic percentages of the films grown under the same conditions the EDX measurements, different ratios are observed in the $W_xFe_{3-x}O_4$ structure (O: 71.05 %, Fe: 4.22 %, W: 24.74 %). The RF power supply seems to be causing more tungsten metal to be sputtered. This is the opposite in the structure of $Ti_xFe_{3-x}O_4$ (O; 58.16 %, Fe; 41.68 %, Ti; 0.17 %). It is possible to say that the power source has an effect here, but also plasma thermodynamics and activation energies of metals play a significant role. The difference in the amount of oxygen in the structures is quite evident. The band gap energy of the as grown and annealing $Ti_xFe_{3-x}O_4$ structures were determined to be 2.19 eV and 2.14 eV respectevily from absorption datas. Same way, as grown and annealing $W_xFe_{3-x}O_4$ structures were determined to be 3.09 eV and 3.15 eV respectevily. When examining the XRD results of the $W_xFe_{3-x}O_4$ crystal monoclinic structure and $Ti_xFe_{3-x}O_4$ polycrystal both orthorhombic and cubic structures are observed. The response of $W_xFe_{3-x}O_4$ structure to hydrogen gas was measured at flow values of 1000 ppm, at 300 degrees, under white light and dark for 300, 180, 120 seconds, and it has been seen that the examined thin films are suitable for gas sensor application under white light. The $W_xFe_{3-x}O_4$ structure exhibits light sensitivity, despite having a relatively wide band gap. However, there is no evidence to suggest that this sensitivity is caused by hydrogen gas; but, it can be sait it is sensitive to light. Also, the response of $Ti_xFe_{3-x}O_4$ structure was measured for 600 seconds, and it has been seen that the examined thin films are not suitable for gas sensor application under white light.

Keywords: $Ti_xFe_{3-x}O_4$, $W_xFe_{3-x}O_4$, gas sensor, magnetron co-sputtering.

Received 8 February 2024; Accepted 4 August 2024.

Introduction

Semi-metallic materials, in which charge carriers exhibit 100 % spin polarization, are highly valuable for promising spintronic device applications. Recent scientific studies aim to develop the structural, magnetic, and transport properties of Fe_3O_4 thin films through doping. In the reverse spinel structure of Fe_3O_4 composition, it was observed that ions such as Mn^{2+} and Zn^{2+} occupied the A sites, while Ti^{4+}, Ni^{2+}, and Co^{2+} ions were found to occupy the octahedral B sites [1-3]. In the past decades, there have been studies on the magnetic properties of the $Fe_{3-x}Ti_xO_4$ structure, particularly in thin film [4-7], nanoparticle [8], and sand-like [9] studies. Non-magnetic Ti-doped Fe_3O_4 ($Fe^{2+}{}_{1+x}Fe^{3+}{}_{2-2x}Ti^{4+}{}_xO_4$, also known as titanomagnetite) is a significant material formed through the substitution of two Fe^{3+} cations with Fe^{2+} and Ti^{4+}. Until now, there has been a lot of uncertainty regarding the ordering of cations in the A and B sites. Some scientific studies show that Ti^{4+} tends to prefer to occupy B sites, resulting in a decrease in magnetic moment with an increase in Ti atomic amount [10-13].

Tungsten oxide (WO_3), which is very useful, is a transition metal oxide known as one of the semiconductors with versatile use, thanks to its polymorphic structure, n-type carrier concentration, band gap energy (~3 eV), light

sensitivity at various wavelengths. It also has good electron mobility and moderate hole diffusion length (~150 nm) [14-17]. From the application point of view, WO3 has distinctive features such as high chemical stability, corrosion resistance, non-toxic, environmentally friendly, abundant in nature, and relatively low cost [14, 16-19]. WO3 is a highly useful material that is widely preferred in various fields, including smart chromogenic windows, photoelectrochemical (PEC) water separation, gas sensing, and photocatalysis [14, 15, 18, 20]. However, it must be modified to meet the needs of the application areas, provide optimal performance, and offer additional features. The primary approach to achieving this goal is to focus on exogenous doping. Doping offers possibilities such as changing the optoelectronic properties of a semiconductor or improving electrical conductivity, and the defect formation and electronic structure modification can be effectively tuned with the help of band gap engineering [14, 15, 17, 21]. It seems quite appropriate to use iron (Fe) metal as an additive to impart suitable optical, electrical, or magnetic properties to tungsten trioxide (WO_3). The most important reason for this compatibility is that Fe and W have similar ionic radii (0.64 Å for Fe^{3+} and 0.62 Å for W^{6+}). This compatibility made Fe metal the most effective additive [16, 22, 23]. Thus, Fe can settle in the regions inside the WO3 crystal [9]. In addition, Fe metal can form oxygen vacancies, which can help lower the electrical resistance and reduce the band gap. Both of these effects are positive and beneficial for gas-sensing applications [23, 24].

Starting with the advancements in the industry, various forms of pollution such as air pollution, water pollution, soil pollution, and environmental pollution have had a negative impact on human life. All subsequent developments also brought about some problems. Harmful gas emissions occur directly or indirectly in various sectors, including technology, health, industry, mineral exploration, space exploration, food production, transportation, and communication. Of course, this situation negatively affects human health and living standards, and it also disrupts the balance that exists in nature. First of all, it is crucial to reduce gas emissions. But there is another situation of equal importance: detecting a flammable, explosive, poisonous, odorless, or tasteless gas accurately and harmlessly within a confined space.

I. Materials and Methods

The changes in many properties such as structural, optical and morphological properties of thin films grown by RF-DC magnetron co-sputter technique after annealing at 550 ^oC were investigated. The response of the thin films obtained to hydrogen gas was measured at a concentration of 1000 ppm (in air+H_2 gas) at a temperature of 300 ^oC.

The $Ti_xFe_{3-x}O_4$ structure and $W_xFe_{3-x}O_4$ structure were grown using the RF-DC magnetron co-sputtering technique. After the films had been grown, X-ray diffraction (XRD), scanning electron microscopy (SEM), and absorption measurements were taken. Subsequently, after annealing hab been performed, and the same measurements were taken again.

First, the substrates were cleaned and placed in the substrate holder. Then, the inside of the sputter chamber was vacuumed to a pressure of $3 \cdot 10^{-6}$ Torr (base pressure). For the $Ti_xFe_{3-x}O_4$ structure, a 2-inch iron target was attached to the DC gun part, while a titanium metal target was attached to the RF gun part. First, plasma was created at 20 mTorr with a flow rate of 100 cubic centimeters per minute (sccm) of argon gas. Then, the substrate temperature was adjusted to 450 ^oC and the rotation speed was set to 3 rotate per minute (rpm). Argon gas was flowing at a rate of 45 sccm, while oxygen gas was flowing at a rate of 5 sccm, resulting in a gassing process that achieved a pressure of 8.4 millitorr inside. After adjusting the power to 50 W for the RF gun and 150 W for the DC gun, growth was carried out for 40 minutes.

Likewise, the entire growth process for $Ti_xFe_{3-x}O_4$ was applied to the $W_xFe_{3-x}O_4$. So, for the $W_xFe_{3-x}O_4$ structure, a 2-inch iron target was attached to the DC gun part, while a tungsten metal target was attached to the RF gun part. First, plasma was created at 20 mTorr with a flow rate of 100 sccm of argon gas. Then, the substrate temperature was adjusted to 450 ^oC and the rotation speed was set to 3 rpm. Argon gas was flowing at a rate of 45 sccm, while oxygen gas was flowing at a rate of 5 sccm, resulting in a gassing process that achieved a pressure of 8.4 millitorr inside. After adjusting the power to 50 W for the RF gun and 150 W for the DC gun, growth was carried out for 40 minutes.

Gas sensor response measurements were tried to be taken with the sensor system that can detect gases and works according to the electrical resistance change mechanism. $Ti_xFe_{3-x}O_4$ and $W_xFe_{3-x}O_4$, H_2 sensor response tests were carried out with the detection system made with a personal design. The gas sensor test system consists of a device with an IV (ampere-volt) measuring probe, a temperature adjustment unit and a precision gas flow meter. For hydrogen sensing application, $Ti_xFe_{3-x}O_4$ and $W_xFe_{3-x}O_4$ temperature was set to 300 °C. Two mass flow controllers are available to achieve dry air and different H_2 ppm levels. All electrical characterization of the sensor was measured with Keithley 487 picoammeter/voltage source under different hydrogen levels and all devices were controlled by electronic command system. In order to take the current-voltage measurement, each sensor measurement cycle was started in a dry air environment. Then 1000 ppm H_2 gas was sent to the gas sensor test chamber, and electric current was measured with a voltage source at a constant voltage of 2 V In this different gas environment.

At higher temperatures, especially when the thermodynamic effect is high, the oxygen ions bound to the surface are more sensitive to the incoming hydrogen gas. Oxygen ions on the surface form H_2O with hydrogen gas above 250 ^oC and leave free electrons at the band gap edge (O^-(ads) + 2H→H_2O + e-), which causes different electrical responses depending on the type of carrier concentration. While these electrons increase the conductivity in n-type material, they decrease the conductivity in a p-type material (h*+ e-→null) [28, 29].

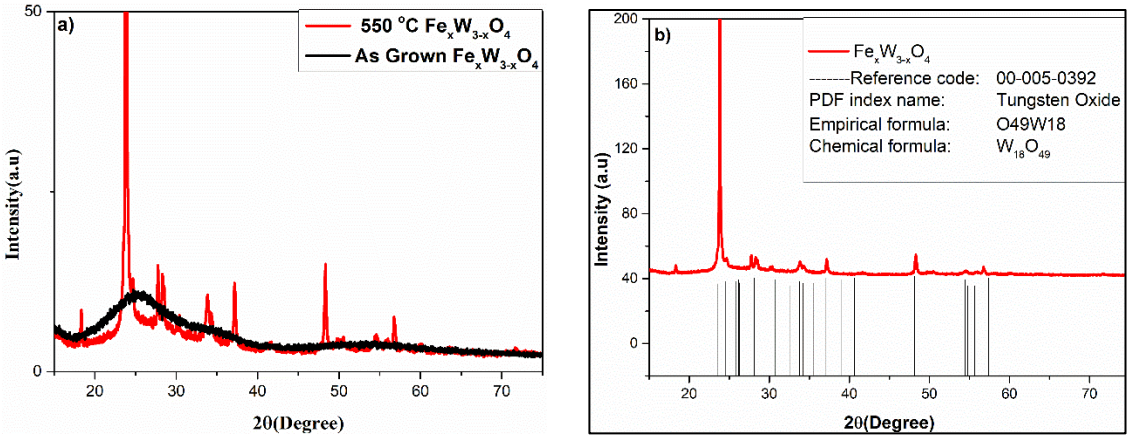

Fig. 1. XRD patterns of **a)** as grown $W_xFe_{3-x}O_4$ and annealed $W_xFe_{3-x}O_4$ at 550°C, **b)** annealed $W_xFe_{3-x}O_4$ at 550°C with XRD reference code.

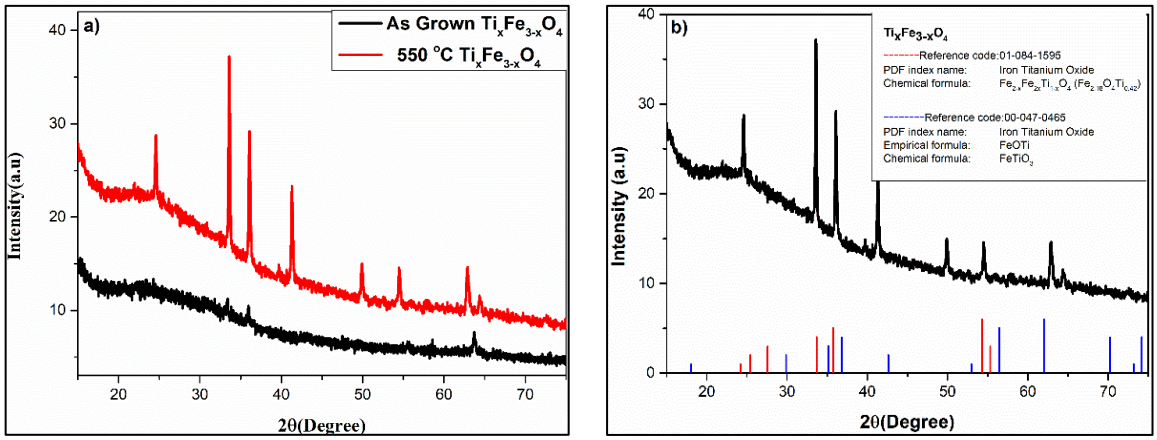

Fig. 2. XRD patterns of **a)** as grown $Ti_xFe_{3-x}O_4$ and annealed $Ti_xFe_{3-x}O_4$ at 550°C, **b)** annealed $Ti_xFe_{3-x}O_4$ at 550°C with XRD reference code.

II. Result and Discussion

In this study, although $Ti_xFe_{3-x}O_4$ and $W_xFe_{3-x}O_4$ compounds were grown under the same conditions, the growth rates of titanium-tungsten metals and the formation of the compounds occurred at different rates. Tungsten metal has a higher growth rate. As evident from the disparities, the thermodynamics of the gas within the growth chamber is intricate and leads to the observation of various amplifications. Parameters such as plasma thermodynamics, metal activation energies, ion radii, crystal lattice substrate compatibility, and substrate temperature seem to influence the dynamics of thin film growth [31, 32].

Another significant finding is that annealing the structure at 550 °C for one hour leads to substantial changes in the XRD, SEM, and absorption results. First of all, while the structures before annealing appear to be in a state close to amorphous, as observed in the XRD results, the characteristic peaks of the structure after annealing are clearly visible. As can be seen from the SEM results, an increase in crystal grain size is observed. While the peaks observed in XRD provide insights into the structural enhancement, the SEM results clearly demonstrate significant improvement. In the absorption results, it is observed that the defects at the edge of the band gap are repaired, and absorption starts at shorter wavelengths. This suggests that the band gap width has increased for $W_xFe_{3-x}O_4$ thin film and also width decreased for $Ti_xFe_{3-x}O_4$ thin film.

When examining the XRD results of the $Ti_xFe_{3-x}O_4$ crystal structure (Fig. 1,a, b), both orthorhombic (Reference code: 00-047-0465) and cubic (Reference code: 01-084-1595) structures are observed. After undergoing a complex process of crystal formation, the emergence of polycrystalline phases is observed.

When examining the XRD results of the annealed $W_xFe_{3-x}O_4$ at 550°C (Fig. 2,a, b) crystal structure monoclinic (Reference code: 00-005-0392) structures are observed. After undergoing a complex process of crystal formation, the emergence of monoclinic phases is observed.

In the calculation made using the data obtained from the absorption measurements (Fig. 3a,3b and Fig. 4a,4b), the band gap energy of the $Ti_xFe_{3-x}O_4$ structure was determined to be 2.19 eV and 2.14 eV after the annealing process. The band gap energy range of the $W_xFe_{3-x}O_4$ structure was calculated to be 3.09 eV before annealing and 3.15 eV after annealing. Fig. 2,b shows the corresponding Tauc plot of the absorption spectra. The

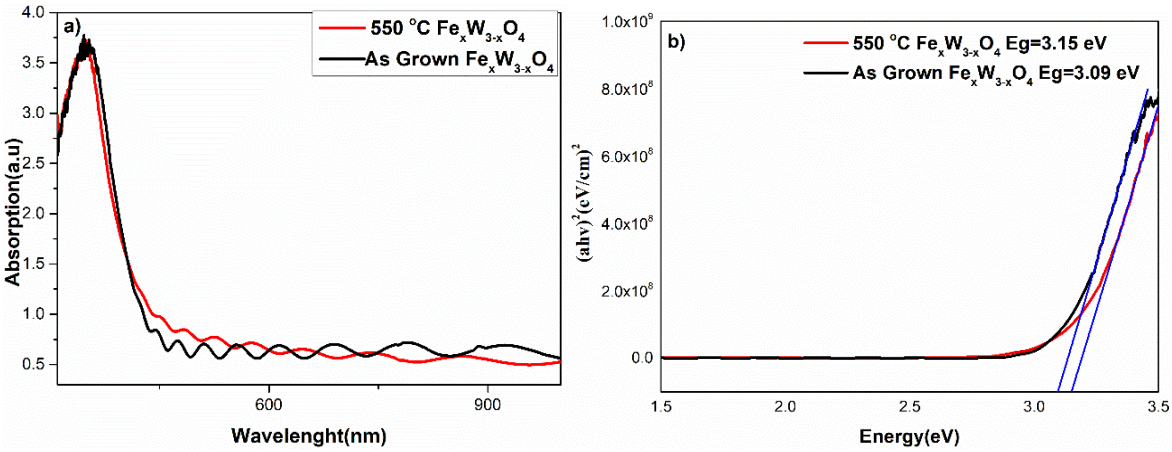

Fig. 3. a) Absorption and **b)** band gap graph of as grown $W_xFe_{3-x}O_4$ and 550 °C annealed $W_xFe_{3-x}O_4$ structure.

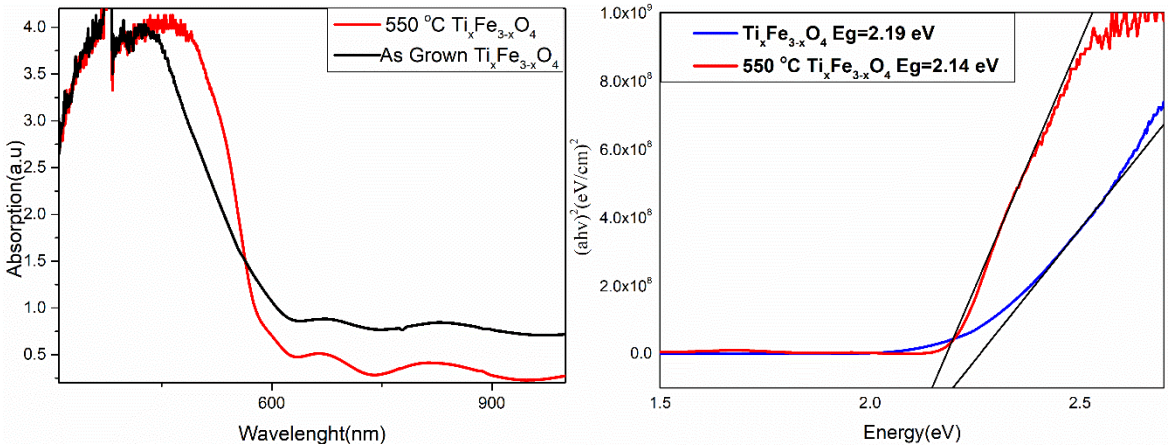

Fig. 4. a) Absorption and **b)** band gap graph of as grown $Ti_xFe_{3-x}O_4$ and 550 °C annealed $Ti_xFe_{3-x}O_4$ structure.

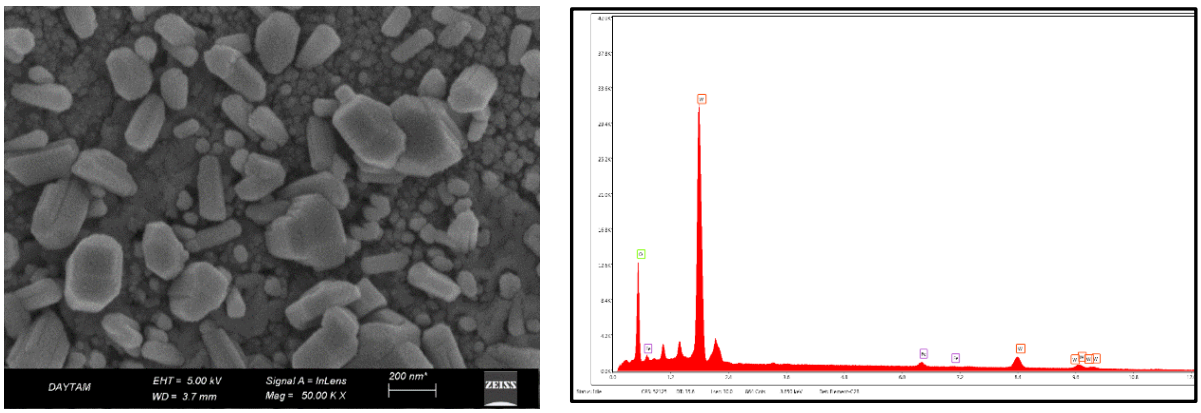

Fig. 5. EDX data and SEM images of the as grown $W_xFe_{3-x}O_4$ and 550 °C annealed $W_xFe_{3-x}O_4$ structure.

direct optical band gap of thin films has been calculated using the Tauc equation.

We can conclude that the calculations of the band gap energy for the $Ti_xFe_{3-x}O_4$ structure and the $W_xFe_{3-x}O_4$ structure highlight the disparity in the incorporation of titanium and tungsten metals within the iron oxide structure. The reactions of the various formations to the annealing process vary significantly from one another. This is due to the difference in the settlement of foreign metals within the structure. Furthermore, the presence of a dominant tungsten oxide structure is observed, even when a lower sputter gun power is used during the growth process. The width of the band gap band of the $W_xFe_{3-x}O_4$ structure indicates the presence of a transparent metal oxide structure.

It was observed that the annealing process led to an increase in crystal grain size, as evident from the SEM images (Fig. 5, 6). Additionally, the XRD results indicated a transition from the amorphous structure to the crystal structure. When examining the atomic percentages of the films grown under identical conditions in the EDX measurements (Fig. 5, 6), different ratios are observed in the $Fe_xW_{3-x}O_4$ structure (O : 71.05 %, Fe: 4.22 %, W: 24.74 %). The RF power supply seems to be causing more tungsten metal to be sputtered. This is the opposite in the structure of $Ti_xFe_{3-x}O_4$ (O; 58.16 %, Fe; 41.68 %, Ti; 0.17 %). It is observed that the 150 W DC power supply transports a significant amount of iron metal, while

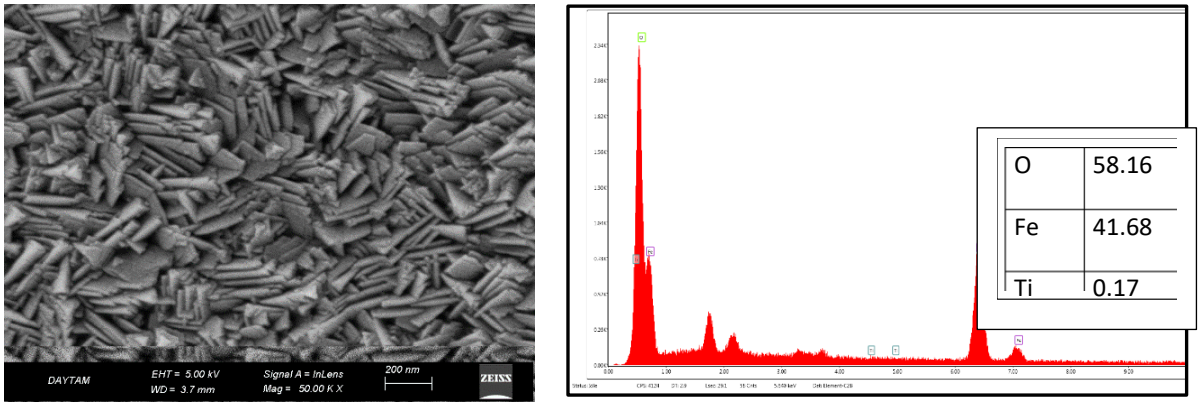

Fig. 6. EDX data and SEM images of the as grown $Ti_xFe_{3-x}O_4$ and 550 ºC annealed $Ti_xFe_{3-x}O_4$ structure.

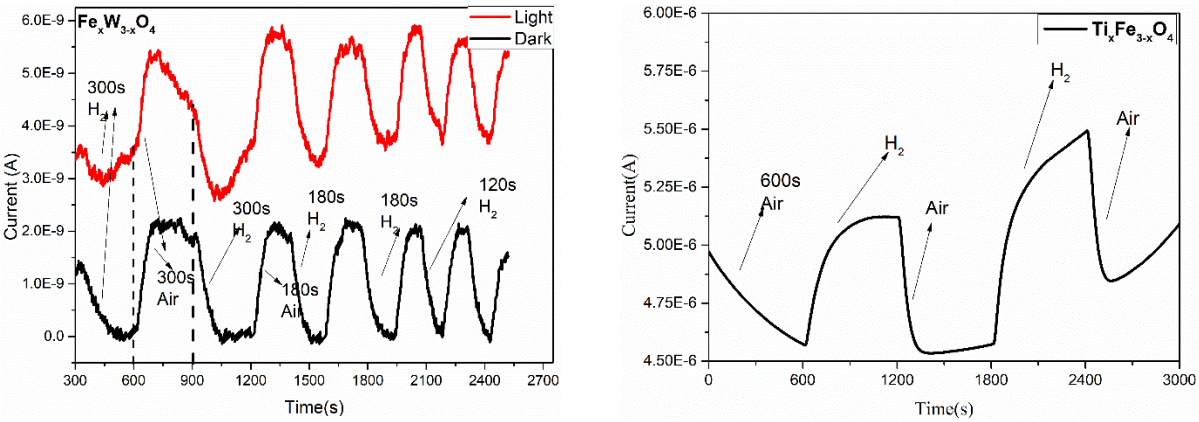

Fig. 7. R sensors response of **a)** $W_xFe_{3-x}O_4$ under white light and dark **b)** 550 ºC annealed $Ti_xFe_{3-x}O_4$ structure for 1000 ppm at 300 ºC.

the 50 W RF power supply transports comparatively less tungsten metal. It is possible to say that the power source has an effect here, but plasma thermodynamics and activation energies of metals play a significant role. The difference in the amount of oxygen in the structures is quite evident.

By giving 99.99 percent pure oxygen gas to the system, it was aimed to clean all gas contamination except the oxygen inside for two hours at 300 ºC by giving high flow oxygen (500 sscm). In addition, the humidity inside was tried to be removed by temperature and oxygen gas flow.

The system is a homemade system and does not have a vacuuming feature, maximum effort is made to provide the most suitable conditions in the measurement system. To obtain different H_2 and dry air ppm level in systems gas, two Alicat Mass Flow Controllers, which are controlling in different flow levels 0 - 0.5 sccm and 0 – 500 sccm, were used and the total flow was fixed to 500 sccm. For the gas sensor measurements, comb-shape interdigitate electrodes (IDT) were fabricated with Ag metal sputtering. The IDT contact distance between electrodes is 500 µm and the total area of the device is 1cm x1cm. The sensor metal, Ag, was sputtered on top of the sample.

The gas sensor measurement was made at 300 degrees at a concentration of 1000 ppm (Fig. 7,a, b) during the same measurement at time intervals such as 600 s, 300 s, 180 s, 120 s.

During gas sensor detection, measurements were re-measured in the dark and under light. In addition, the results were compared with the other gas sensor measure (Fig. 7,b) in order to understand how the Ti, W elements affect the gas sensor detection. According to the electrical resistance change mechanism, the gas sensor response was made according to the equation [%R = (Io-I\Io)·100]. Here, R is sensors response. I_0 is first current, and I is finally current.

As it can be understood from the gas sensor measurements (in Fig. 7,a), it can be said that the 550 ºC annealed $W_xFe_{3-x}O_4$ structure is a semiconductor with a p-type carrier concentration. When the hydrogen gas introduced during the gas sensor measurement connects the oxygens to itself, the electrons remaining in the crystal structure combine in the halls and the conductivity decreases, that is, the measured current decreases [30]. So, the bending of the conduction and valence bands caused by gas molecules is responsible for the change in conductivity.

For unannealed $W_xFe_{3-x}O_4$ thin film, the carrier concentration decreases because electrons lost as a result of the reaction $2H_2 + O^{-2}$ (ads)$\rightarrow 2H_2O + e-$ combine with the holes. Thus, the current decreases [34].

Also as it can be understood from the gas sensor measurements (in Fig. 7,b), it can be said that the 550 ºC annealed $Ti_xFe_{3-x}O_4$ thin film is a semiconductor with a n-type carrier concentration. When the hydrogen gas introduced during the gas sensor measurement connects the oxygens to itself, the electrons remaining in the crystal structure and the film conductivity in creases, that is, the measured current increases [30]. For unannealed $W_xFe_{3-x}O_4$ thin film, the carrier concentration decreases because

electrons lost as a result of the reaction $2H_2 + O^{-2}$ (ads)$\rightarrow 2H_2O + e-$ and carrier concentration increases with the electrons. Thus, the current increases [33, 35].

The sensor responses achieved are R_f = 1100 %, 73 % for the $Ti_xFe_{3-x}O_4$, $W_xFe_{3-x}O_4$ respectly (Fig. 7,a, b). The response times of the sensor are 598 s, 168 s and the recovery times are 155 s,172 s. for the $Ti_xFe_{3-x}O_4$, $W_xFe_{3-x}O_4$ respectly (Fig. 7,a, b). It is seen that the recovery time of $Ti_xFe_{3-x}O_4$ is shortened, and it also showed the highest response to a relative gas concentration of 1000 ppm. It is seen that the surface is sensitive to oxygen, the substrate positively affects the structure and shows that it can be developed as a suitable material for the gas sensor.

Conclusion

Finally, in the EDX measurements, different ratios are observed in the $W_xFe_{3-x}O_4$ structure (O: 71.05 %, Fe: 4.22 %, W: 24.74 %). The RF power supply seems to be causing more tungsten metal to be sputtered. This is the opposite in the structure of $Ti_xFe_{3-x}O_4$ (O; 58.16 %, Fe; 41.68 %, Ti; 0.17 %). It is observed that the 150 W DC power supply transports a significant amount of iron metal, while the 50 W RF power supply transport comparatively less tungsten metal. It is possible to say that the power source has an effect here, but plasma thermodynamics and activation energies of metals play a significant role. The difference in the amount of oxygen in the structures is quite evident.

The response of $W_xFe_{3-x}O_4$ structure grown by RF-DC co-sputtering to hydrogen gas was measured at flow values of 1000 ppm, at 300 degrees and under white light in the same cycle for 300, 180, 120 seconds, and it has been seen that the examined thin films are suitable for gas sensor application under white light. The $W_xFe_{3-x}O_4$ structure exhibits light sensitivity, despite having a relatively wide band gap. However, there is no evidence to suggest that this sensitivity is caused by hydrogen gas; but, it can bu said it is sensitive to light.

The response of $Ti_xFe_{3-x}O_4$ structure grown by RF-DC co-sputtering to hydrogen gas was measured at flow values of 1000 ppm, at 300 °C and under white light in the same cycle for 600 seconds, and it has been seen that the examined thin films are not suitable for gas sensor application under light. Also, no change was observed in the sensor response of the structure in the dark so it is not sensitive to light.

Acknowledgment

The research conducted in this study received financial support from Ataturk University. The author would like to express gratitude to Eastern Anatolia High Technology Application and Research Center (DAYTAM) for their valuable assistance. The authors would like to thank the Atatürk University Scientific Research Projects Coordination Department under the Grant No. FBA-2023-11526 for the supports.

Erdal Turgut *– Atatürk University, Department of Electric Power Generation, Aşkale Vocational College, Erzurum, Turkey;*
Elvan Şenarslan *– Atatürk University, Department of Electric Power Generation, Aşkale Vocational College, Erzurum, Turkey;*
Günay Merhan Muğlu *– Atatürk University, Department of Medical Services and Techniques, Hınıs Vocational School, Erzurum, Turkey, gunay.merhan@atauni.edu.tr*
Sevda Sarıtaş *– Atatürk University, Department of Electric Power Generation, Transmission and Distribution, İspir Hamza Polat Vocational College, Erzurum, Turkey, sevda.saritas@atauni.edu.tr*

[1] A. Chanda, C.M. Hung, A.T. Duong, S. Cho, H. Srikanth, & M.H. Phan, *Magnetism and spin-dependent transport phenomena across Verwey and Morin transitions in iron oxide/Pt bilayers*, Journal of Magnetism and Magnetic Materials, 568, 170370 (2023); https://doi.org/10.1016/j.jmmm.2023.170370.

[2] J.A. Peters, *Relaxivity of manganese ferrite nanoparticles.* Progress in Nuclear Magnetic Resonance Spectroscopy, 120, 72 (2020); https://doi.org/10.1016/j.pnmrs.2020.07.002.

[3] D. Varshney, A. Yogi, K. Verma & D.M. Phase, *Transport Properties of $Fe_{3-x}Ti_xO_4$ (x = 0.0 and 0.0206) Epitaxial Thin Films*, In AIP Conference Proceedings, American Institute of Physics, 1349(1), 599 (2011); https://doi.org/10.1063/1.3606000.

[4] H. Yamahara, M. Seki, M. Adachi, M. Takahashi, H. Nasu, K. Horiba, & H. Tabata, *Spin-glass behaviors in carrier polarity controlled $Fe_{3-x}Ti_xO_4$ semiconductor thin films*, Journal of Applied Physics, 118(6), (2015); https://doi.org/10.1063/1.4928408.

[5] D. Varshney, A.Yogi, *Structural, transport and spectroscopic properties of Ti^{4+} substituted magnetite: $Fe_{3-x}Ti_xO_4$*, Materials Chemistry and Physics, *133*(1), 103-109, (2012); https://doi.org/10.1016/j.matchemphys.2011.12.068.

[6] C. Jin, W.B. Mi, P. Li, & H.L. Bai, *Experimental and first-principles study on the magnetic and transport properties of Ti-doped Fe_3O_4 epitaxial films*, Journal of Applied Physics, 110(8), (2011); https://doi.org/10.1063/1.3650252.

[7] T.C. Droubay, C.I. Pearce, E.S. Ilton, M.H. Engelhard, W. Jiang, S.M. Heald, & K.M. Rosso, *Epitaxial $Fe_{3-x}Ti_xO_4$ films from magnetite to ulvöspinel by pulsed laser deposition*, Physical Review B, 84(12), 125443 (2011); https://doi.org/10.1103/PhysRevB.84.125443.

[8] D. Azarifar, R. Asadpoor, O. Badalkhani, M. Jaymand, E. Tavakoli, & M. Bazouleh, *Sulfamic-Acid-Functionalized $Fe_{3-x}Ti_xO_4$ Nanoparticles as Novel Magnetic Catalyst for the Synthesis of Hexahydroquinolines under Solvent-Free Condition*, ChemistrySelect, 3(48), 13722 (2018); https://doi.org/10.1002/slct.201802505.

[9] S. Sunaryo, & I. Sugihartono, *Separation Study of Titanomagnetite $Fe_{3-x}Ti_xO_4$ from Natural Sand at Indramayu, West Java*, Makara Journal of Technology, 14(2), 106 (2011); https://doi.org/10.7454/mst.v14i2.701.

[10] C. Jin, W.B. Mi, P. Li, & H.L. Bai, *Experimental and first-principles study on the magnetic and transport properties of Ti-doped Fe_3O_4 epitaxial films*, Journal of Applied Physics, 110(8), (2011); https://doi.org/10.1063/1.3650252.

[11] A. Kosterov, L. Surovitskii, V. Maksimochkin, S. Yanson, & A. Smirnov, *Tracing titanomagnetite alteration with magnetic measurements at cryogenic temperatures*, Geophysical Journal International, 235(3), 2268 (2023); https://doi.org/10.1093/gji/ggad360.

[12] P.V. Kharitonskii, Y.A. Anikieva, N.A. Zolotov, K.G. Gareev, & A.Y. Ralin, *Micromagnetic modeling of Fe_3O_4–$Fe_{3-x}Ti_xO_4$ composites*, Physics of the Solid State, 64(9), (2022); https://doi.org/10.21883/pss.2022.09.54172.31hh.

[13] F. Bosi, U. Hålenius & H. Skogby, *Crystal chemistry of the magnetite-ulvospinel series*, American Mineralogist, 94(1), 181 (2009); https://doi.org/10.2138/am.2009.3002.

[14] T. Zhang, Z. Zhu, H. Chen, Y. Bai, S. Xiao, X. Zheng & S. Yang, *Iron-doping-enhanced photoelectrochemical water splitting performance of nanostructured WO_3: a combined experimental and theoretical study*,Nanoscale, 7(7), 2933 (2015); https://doi.org/10.1039/c4nr07024k.

[15] D. Ilager, H. Seo, N.P. Shetti, & S.S. Kalanur, *CTAB modified Fe-WO_3 as an electrochemical detector of amitrole by catalytic oxidation*, Journal of Environmental Chemical Engineering, 8(6), 104580 (2020); https://doi.org/10.1016/j.jece.2020.104580.

[16] M.T. Merajin, M. Nasiri, E. Abedini & S. Sharifnia, *Enhanced gas-phase photocatalytic oxidation of n-pentane using high visible-light-driven Fe-doped WO_3 nanostructures*, Journal of environmental chemical engineering, 6(5), 6741 (2018); https://doi.org/10.1016/j.jece.2018.10.037.

[17] K. Song, Z. Ma, W. Yang, H. Hou, & F. Gao, *Electrospinning WO_3 nanofibers with tunable Fe-doping levels towards efficient photoelectrochemical water splitting*, Journal of Materials Science: Materials in Electronics, 29, 8338 (2018); https://doi.org/10.1007/s10854-018-8844-3.

[18] C.C. Mardare, & A.W. Hassel, *Review on the versatility of tungsten oxide coatings*, Physica status solidi (a), 216(12), 1900047 (2019); https://doi.org/10.1002/pssa.201900047.

[19] M.B. Tahir, G. Nabi, N.R. Khalid, & W.S. Khan, *Synthesis of nanostructured based WO_3 materials for photocatalytic applications*, Journal of Inorganic and Organometallic Polymers and Materials, 28, 777 (2018); https://doi.org/10.1007/s10904-017-0714-6.

[20] S. Ramkumar, & G. Rajarajan, *Effect of Fe doping on structural, optical and photocatalytic activity of WO_3 nanostructured thin films*, Journal of Materials Science: Materials in Electronics, 27, 1847 (2016); https://doi.org/10.1007/s10854-015-3963-6.

[21] Z. Zhang, Z. Wen, Z. Ye, & L. Zhu, *Ultrasensitive ppb-level NO2 gas sensor based on WO3 hollow nanosphers doped with Fe*, Applied Surface Science, 434, 891 (2018); https://doi.org/10.1016/j.apsusc.2017.10.074.

[22] M. Ahsan, T. Tesfamichael, M. Ionescu, J. Bell, & N. Motta, *Low temperature CO sensitive nanostructured WO3 thin films doped with Fe*, Sensors and Actuators B: Chemical, 162(1), 14 (2012); https://doi.org/10.1016/j.snb.2011.11.038.

[23] F. Mehmood, J. Iqbal, T. Jan, & Q. Mansoor, *Structural, Raman and photoluminescence properties of Fe doped WO_3 nanoplates with anti cancer and visible light driven photocatalytic activities*, Journal of Alloys and Compounds, 728, 1329 (2017); https://doi.org/10.1016/j.jallcom.2017.08.234.

[24] J.C. Wang, W. Shi, X.Q. Sun, F.Y. Wu, Y. Li, & Y. Hou, *Enhanced Photo-Assisted Acetone Gas Sensor and Efficient Photocatalytic Degradation Using Fe-Doped Hexagonal and Monoclinic WO_3 Phase – Junction*, Nanomaterials, 10(2), 398 (2020); https://doi.org/10.3390/nano10020398.

[25] A. Paleczek, D. Grochala, K. Staszek, S. Gruszczynski, E. Maciak, Z. Opilski & A. Rydosz, *An NO_2 sensor based on WO_3 thin films for automotive applications in the microwave frequency range*, Sensors and Actuators B: Chemical, 376, 132964 (2023); https://doi.org/10.1016/j.snb.2022.132964.

[26] S. Hambir, & S. Jagtap, *Nitrogen dioxide gas-sensing properties of hydrothermally synthesized $WO_3{\cdot}nH_2O$ nanostructures*, Royal Society Open Science. 10(4), 221135 (2023); https://doi.org/10.1098/rsos.221135.

[27] Y.C. Chiu, M. Deb, P.T. Liu, H.W. Zan, Y.R. Kuo Y. Shih & C.C. Hsu, *Sputtered Ultrathin WO_3 for Realizing Room-Temperature High-Sensitive NO_2 Gas Sensors*, ACS Applied Electronic Materials 5(11), 5831 (2023); https://doi.org/10.1021/acsaelm.3c00725.

[28] Ruiyang Miao, Wen Zeng, Qi Gao, *SDS-assisted hydrothermal synthesis of NiO flake-flowerarchitectures with enhanced gas-sensing properties*, Appl. Surf. Sci. 384, 304 (2016); https://doi.org/10.1016/j.apsusc.2016.05.070.

[29] S. Saritas, M. Kundakci, O. Coban, S. Tuzemen, M. Yildirim, *Ni: Fe_2O_3, Mg: Fe_2O_3 and Fe_2O_3 thin films gas sensor application*, Physica B: Condensed Matter, 541, 14 (2018); ISSN 0921-4526; https://doi.org/10.1016/j.physb.2018.04.028.

[30] T. Manoj, H.P. Perumal, B. Paikaray, A. Haldar, J. Sinha, P.P. Bhattacharjee & C. Murapaka, *Perpendicular magnetic anisotropy in a sputter deposited nanocrystalline high entropy alloy thin film*, Journal of Alloys and Compounds, 930, 167337 (2023); https://doi.org/10.1016/j.jallcom.2022.167337.

[31] A. Bahr, S. Richter, R. Hahn, T. Wojcik, M. Podsednik, A. Limbeck & H. Riedl, *Oxidation behaviour and mechanical properties of sputter-deposited TMSi$_2$ coatings (TM= Mo, Ta, Nb)*, Journal of Alloys and Compounds, 931, 167532 (2023); https://doi.org/10.1016/j.jallcom.2022.167532.

[32] S.G. Khalil, & M.M. Mutter, *Synthesis and Characterization of Semiconductor Composites Gas Sensors Based on ZnO Doped TiO$_2$ Thin Films by Laser-Induced Plasma*, Key Engineering Materials, 900, 112 (2021); https://doi.org/10.4028/www.scientific.net/KEM.900.112.

[33] Z. Qu, Y. Li, R. Xu, C. Li, H. Wang, & Q. Wei, *Candy-like heterojunction nanocomposite of WO$_3$/Fe$_2$O$_3$-based semiconductor gas sensor for the detection of triethylamine*, Microchimica Acta, 190(4), 139 (2023); https://doi.org/10.1007/s00604-023-05699-x.

[34] D. Wang, S. Giannakis, J. Tang, K. Luo, J. Tang, Z. He, & L. Wang, *Effect of rGO content on enhanced Photo-Fenton degradation of Venlafaxine using rGO encapsulated magnetic hexagonal FeTiO$_3$ nanosheets*, Chemical Engineering Journal, 478, 147319 (2023); https://doi.org/10.1016/j.cej.2023.147319.

Ердал Тургут[1], Ельван Шенарслан[1], Гюнай Мерхан Муглу[2], Севда Сарітас[3]

Дослідження титано-вольфрамового оксиду заліза як датчика газу

[1]Університет Ататюрка, кафедра генерації електроенергії, Ерзурум, Туреччина;
[2]Університет Ататюрка, факультет медичних послуг і техніки, Туреччина;
[3]Університет Ататюрка, кафедра виробництва, передачі та розподілу електроенергії, Ерзурум, Туреччина, sevda.saritas@atauni.edu.tr

Отримано структури $Ti_xFe_{3-x}O_4$ та $W_xFe_{3-x}O_4$. При зміні атомного відсотка плівок, вирощених за тих самих умов, за результатами EDX аналізу, спостерігаються різні співвідношення в їх структурі: $W_xFe_{3-x}O_4$(O: 71,05 %, Fe: 4,22 %, W: 24,74 %) та $Ti_xFe_{3-x}O_4$ (O; 58,16 %, Fe; 41,68 %, Ti; 0,17 %). Можна сказати, що тут є внесок джерела живлення, але істотну роль відіграють також термодинаміка плазми та енергія активації металів. Різниця в кількості кисню у цих структурах є очевидна. Енергія забороненої зони вирощеної та відпаленої структур $Ti_xFe_{3-x}O_4$ була визначена з даних поглинання як 2,19 еВ та 2,14 еВ, відповідно. Отритмано, що під час вирощування та відпалу структури для $W_xFe_{3-x}O_4$ ці значення становлять 3,09 еВ і 3,15 еВ, відповідно. При дослідженні результатів XRD моноклінної структури кристала $W_xFe_{3-x}O_4$ і полікристала $Ti_xFe_{3-x}O_4$ спостерігаються як ромбічні, так і кубічні структури. Відповідь структури $W_xFe_{3-x}O_4$ на газоподібний водень вимірювали при значеннях потоку 1000 ppm, при 300 градусах, під білим світлом і темрявою протягом 300, 180, 120 секунд, і було видно, що розглянуті тонкі плівки придатні для газу застосування датчика під білим світлом. Структура $W_xFe_{3-x}O_4$ проявляє світлочутливість, незважаючи на відносно широку заборонену зону. Однак немає доказів того, що ця чутливість спричинена газоподібним воднем; але можна твердити про чутливість до освітлення. Крім того, відповідь структури $Ti_xFe_{3-x}O_4$ вимірювали протягом 600 секунд, і було видно, що досліджувані тонкі плівки не підходять для застосування у якості газового датчика під дією білого світла.

Ключові слова: $Ti_xFe_{3-x}O_4$, $W_xFe_{3-x}O_4$, датчик газу, магнетронне напилення.